*International Immunology, Vol. 33, No. 5, pp. 281–298*
doi:10.1093/intimm/dxab003
Advance Access publication 6 January 2021

*© The Author(s) 2021. Published by Oxford University Press on behalf of The Japanese Society for Immunology. All rights reserved. For permissions, please e-mail: journals.permissions@oup.com*

# Modeling the immune response to *Salmonella* during typhoid

**Divy Dhingra[1,*], Sandhya Amol Marathe[2,*], Nandita Sharma[2], Amol Marathe[1]** and **Dipshikha Chakravortty[3]**

[1]Department of Mechanical Engineering and
[2]Department of Biological Sciences, Birla Institute of Technology & Science, Pilani, Rajasthan 333031, India
[3]Department of Microbiology and Cell Biology, Indian Institute of Science, Bangalore, Karnataka 560012, India

*Correspondence to*: S. A. Marathe; E-mail: sandhya.marathe@pilani.bits-pilani.ac.in or D. Dhingra; E-mail: dhingra.divy@gmail.com

*These authors contributed equally to this study.

*Received* 12 August 2020, *editorial decision* 1 January 2021; *accepted* 5 January 2021

**Several facets of the host immune response to *Salmonella* infection have been studied independently at great depths to understand the progress and pathogenesis of *Salmonella* infection. The circumstances under which a *Salmonella*-infected individual succumbs to an active disease, evolves as a persister or clears the infection are not understood in detail. We have adopted a system-level approach to develop a continuous-time mechanistic model. We considered key interactions of the immune system state variables with *Salmonella* in the mesenteric lymph node to determine the final disease outcome deterministically and exclusively temporally. The model accurately predicts the disease outcomes and immune response trajectories operational during typhoid. The results of the simulation confirm the role of anti-inflammatory ($M_2$) macrophages as a site for persistence and relapsing infection. Global sensitivity analysis highlights the importance of both bacterial and host attributes in influencing the disease outcome. It also illustrates the importance of robust phagocytic and anti-microbial potential of $M_1$ macrophages and dendritic cells (DCs) in controlling the disease. Finally, we propose therapeutic strategies for both antibiotic-sensitive and antibiotic-resistant strains (such as IFN-γ therapy, DC transfer and phagocytic potential stimulation). We also suggest prevention strategies such as improving the humoral response and macrophage carrying capacity, which could complement current vaccination schemes for enhanced efficiency.**

*Keywords:* active disease, clearance, latency, mesenteric lymph node

## Introduction

Every year, approximately 14.3 million individuals suffer from typhoid fever, with 136 000 estimated deaths worldwide (1). The majority of the cases and deaths (~72%) are from Asiatic countries (1). Of the infected individuals, 1–6% suffer from recurrent infection and a similar number of infected individuals act as asymptomatic carriers (2). However, it is still not clear what leads to the development of the carrier (persister) state or clearance of infection. Whether it is the immune state of the host at the time of infection or the action of different virulence factors (of *Salmonella*) that determines the progress of infection has not been fully investigated. Human typhoid infection is caused by *Salmonella enterica* subspecies *enterica* serovar Typhi, which is restricted to humans, making it difficult to study its pathogenesis with available animal models (except non-human primates like chimpanzees) (3). Murine typhoid caused by *S. enterica* subsp. *enterica* serovar Typhimurium is very similar to human typhoid and has been successfully used to study various aspects of typhoid fever (3), including persistence of infection (4). Thus, we base our study on a murine model of typhoid fever.

For murine typhoid, the response following first exposure to *S. enterica* serovar Typhimurium usually initiates in the Peyer's patches (PPs) and mesenteric lymph node (MLN). The MLN acts as a restrictive site restraining the systemic spread of *Salmonella* (5). In the MLN, some bacteria establish a non-replicating population (persisters) inside macrophages, probably acting as a source of relapsing infection (6). What triggers the development of these persisters is only partially understood. It has been proposed that IFN-γ keeps the infected macrophages activated (pro-inflammatory macrophages) and its neutralization leads to the relapse of *Salmonella* infection, suggesting the role of a $T_{H1}$ response in maintaining the persistent state (4). The IFN-γ- and TNF-α-activated macrophages are referred to as classically

Downloaded from https://academic.oup.com/intimm/article/33/5/281/6066543 by guest on 27 December 2022

activated or $M_1$ macrophages (7). These macrophages exhibit a strong anti-microbial activity, and the ability to damage tissue and enhance $T_{H1}$ responses *via* IL-12 production (7). On the other hand, the macrophages activated by IL-4, IL-10 or IL-13, termed as alternatively activated or $M_2$ macrophages, resolve inflammation, alleviate tissue damage and promote $T_{H2}$ responses (7) by secreting anti-inflammatory cytokines. In a mouse model of persistent *Salmonella* infection, bacteria were preferentially associated with anti-inflammatory $M_2$ macrophages and required $T_{H2}$-mediated signaling (8). *Salmonella* infection polarizes the macrophages toward the anti-inflammatory $M_2$ type (9). Even though the importance of $M_2$ macrophages is well established, we cannot rule out the role of other immune components, such as dendritic cells (DCs), T cells and cytokines, in governing the disease progression. For example, IFN-γ activates DCs and macrophages (converting them into $M_1$ macrophages) by increasing the expression of co-stimulatory molecules (10, 11), which is critical to the resolution of *Salmonella* infection (12).

The migrating $CCR6^+$ DCs in MLN and PPs are important in activating $CD4^+$ T cells. Proper functioning of IFN-γ- and IL-12-dependent immunity is crucial for eliminating *Salmonella* from the reticuloendothelial system (13).

Various aspects of the host immune response to *Salmonella* infection have been modeled, such as *Salmonella* colonization dynamics in cecal lymph node using a stochastic birth–death–immigration model (14, 15) and within host spatiotemporal population dynamics in different organs such as liver and spleen (16). However, we did not come across any literature studying the interactions of the immune system components, such as macrophages, $T_{H1}$ and $T_{H2}$ cells, DCs, and cytokines IFN-γ, IL-12 and IL-4, with *Salmonella* at an organ level that determines the final disease outcome deterministically and temporally. In the present study, we model the progress of *Salmonella* pathogenesis in the MLN as temporal evolution of the state of a dynamical system comprising key cellular–cytokine interactions as well as cytokine–cytokine cross-regulation.

## Methods

### *Model development*

Because of the dearth of information on immune response studies with *S. enterica* subsp. *enterica* serovar Typhi, we use the data on murine typhoid to develop the model and obtain quantitative estimates of variables and parameters for our model. During murine typhoid, the immunological processes active in the MLN are crucial in determining the final fate of *Salmonella* infection (5, 17). In chronically infected mice (latent carriers), some bacteria establish a non-replicating population (called persisters) inside anti-inflammatory macrophages ($M_2$ type) present in the MLN and are considered as the source of relapsing infection (4, 8). We, therefore, consider the MLN as a reference space to model the progress of *Salmonella* pathogenesis. We develop a network describing key pathways such as cellular–cytokine, cell–cell interactions and cytokine–cytokine cross-regulation (Fig. 1). Fundamentals of this interaction network are described in the next paragraph. On the basis of the network generated, we develop a continuous-time mechanistic model consisting of a system of 20 first-order non-linear ordinary differential equations (Equations 1–20, Supplementary Methods) by considering different types of macrophages, T lymphocytes, cytokines and bacterial populations from the interaction network as the model variables. The mathematical details of the model are provided in the Supplementary Methods. Key model assumptions are as follows:

- Only the extracellular bacteria ($B_E$) are able to stimulate DCs and macrophages to produce cytokines, while intracellular bacteria have negligible effect.
- Self-proliferating cells follow logistic growth.
- Cellular and cytokine dynamics is governed by the laws of enzyme kinetics.
- Michaelis–Menten kinetics is used to describe the rates that are limited by the cell density or cytokine concentration.
- Multi-substrate kinetics is used if the rate is affected by the concentrations of two variables.

DCs and macrophages (especially $M_1$ type) play a crucial role in controlling the *Salmonella* infection (18, 19). The phagocytic cells used for model development include immature and mature ($DC_{im}$ and $DC_m$, respectively) DCs, and resting ($M_0$, representing macrophages that are not activated), pro-inflammatory ($M_1$) and anti-inflammatory ($M_2$) macrophages. We depict the conversion, recruitment and infection processes of these cells in Fig. 1. DCs act as sentinel cells sampling *Salmonella* from the gut as well as PPs and migrate to the MLN (20). The cytokines IL-12, IFN-γ and IL-4 govern the conversion mechanisms of phagocytes (10, 19). As shown in Fig. 1(A), IFN-γ stimulates the maturation of $DC_{im}$ to $DC_m$, and an interplay between IFN-γ and IL-4 regulates the polarization of macrophages to $M_1$ and $M_2$ types, respectively. *Salmonella* infection in the MLN triggers further recruitment of macrophages (Fig. 1B) (18) and induces death of some infected phagocytes (Fig. 1A and B) (21, 22). The infected macrophages also die of natural killer (NK) cell-induced lysis (Fig. 1B) (23). We consider T lymphocytes, specifically naive T cells ($T_{HN}$) and $CD4^+$ T cells ($T_{H0}$, $T_{H1}$ and $T_{H2}$), for the model development. The kinetics of $T_H$ lymphocytes in the MLN during typhoid is summarized in Fig. 1(C). The $T_{HN}$ cells are continuously recirculated in and out of the MLN (24) and are recruited by activated DCs (Fig. 1C). DCs present antigens to these recirculating $T_{HN}$ cells, thereby converting them into precursor T cells ($T_{H0}$). Depending on the relative concentration of the key $T_{H1}$ cytokines (IL-12 and IFN-γ) and the $T_{H2}$ cytokine (IL-4), the $T_{H0}$ cells differentiate to either $T_{H1}$ or $T_{H2}$ type. $T_H$ lymphocytes play a crucial role in developing an immune response against *Salmonella*. Infected DCs activate *Salmonella*-specific $CD4^+$ T lymphocytes triggering their proliferation (Fig. 1C) (25). The pro-inflammatory (IFN-γ) and anti-inflammatory (IL-4) cytokines secreted by the $T_H$ cells modulate the functions of various immune cells to heal tissue damage and control the spread of infection. Hence, the balance of $T_{H1}/T_{H2}$ response is crucial in determining the fate (active disease, latency or clearance) of *Salmonella* infection (26, 27). The potential of host and bacteria to counter each other influences the severity and outcome of *Salmonella* infection. The cytokines act as key regulators in the bacteria–host

Downloaded from https://academic.oup.com/intimm/article/33/5/281/6066543 by guest on 27 December 2022

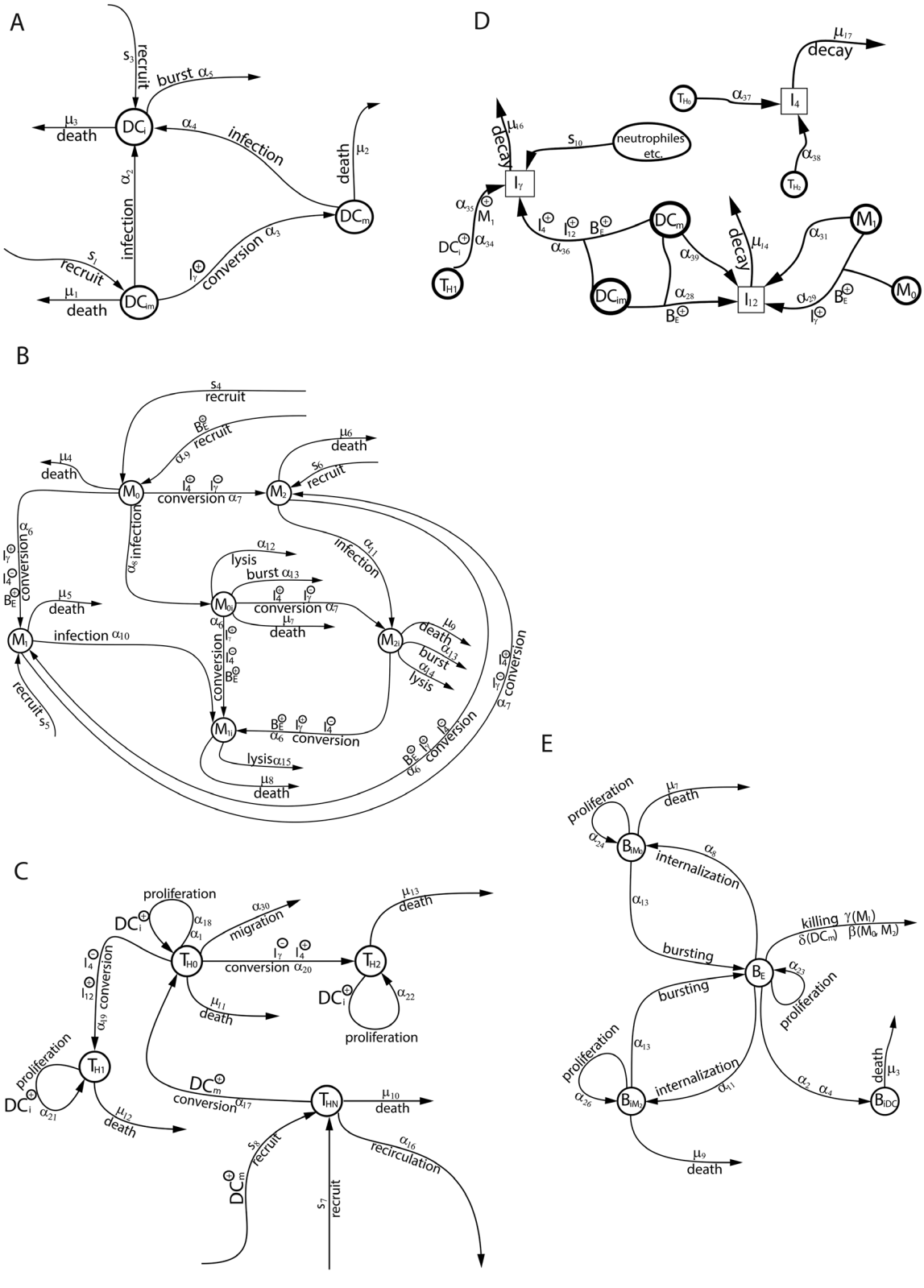


**Fig. 1.** Immune cells, cytokines and bacterial interaction networks for model development. (A, B) Phagocyte interaction network. (A) The recruitment, conversion and infection kinetics of three types of dendritic cell (DC) populations—immature DC ($DC_{im}$), mature DC ($DC_m$) and infected DC ($DC_i$)—are represented. (B) Macrophage recruitment, conversion and infection kinetics along with lymphocyte-mediated lysis is represented. Six types of macrophages—resting ($M_0$), pro-inflammatory ($M_1$) and anti-inflammatory ($M_2$), and their infected counterparts ($M_{0i}$, $M_{1i}$

Downloaded from https://academic.oup.com/intimm/article/33/5/281/6066543 by guest on 27 December 2022

interactions. The bacterial components trigger the production and secretion of chemokines and cytokines by immune cells influencing the hosts' potential to clear the infection. As discussed above, the chemokines and cytokines orchestrate the recruitment, proliferation, conversion/differentiation and activation of immune cells to control the infection. We consider three key cytokines, IL-12, IFN-γ and IL-4, while developing the model for typhoid. IFN-γ plays an important role in the progress of *Salmonella* infection by inducing systemic inflammation and immune cell activation (12). As depicted in Fig. 1(D), $B_E$ induces the secretion of inflammatory cytokines, IL-12 and IFN-γ by DCs (28). IL-12 and IL-4 enhance the IFN-γ production by DCs (29). IL-12 is also produced by macrophages (28) and IFN-γ significantly enhances its secretion (Fig. 1D). Neutrophils along with NK and $CD8^+$ T cells secrete IFN-γ as a function of IL-12 (Fig. 1E). DCs and $M_1$ macrophages stimulate $T_{H1}$ cells to secrete IFN-γ (25, 30). IL-4 is primarily secreted by $T_{H0}$ and $T_{H2}$, and it plays a role in macrophage and $T_H$-cell differentiation.

*Salmonella* reach the MLN either as extracellular bacteria ($B_E$) or as intracellular bacteria within DCs (infected DC [$DC_i$]) (20). The pathogenic potential of *Salmonella* is one of the important factors deciding the progress of typhoid fever. We depict the proliferation, conversion and killing dynamics for extracellular ($B_E$) and intracellular ($B_I$) bacteria in Fig. 1(E). The phagocytosis of extracellular bacteria by macrophages and DCs is represented as internalization in Fig. 1(E).

### *Model simulation*

*Initial conditions and parameter estimation.* Immune response to the *Salmonella* progression is modeled as an initial value problem. We deduce relevant values for initial conditions (ICs) and ranges for model parameters from the literature on murine typhoid using methods described by Wigginton *et al.* (31) (Supplementary Methods). For those not obtained through literature, the mean and standard deviation of the output data of *in vivo* and *in vitro* experiments performed in this study are used to deduce the same (Supplementary Methods). The units of ICs and parameters are per milliliter of MLN for cells and bacteria, and picogram per milliliter of MLN for cytokines. ICs for the host variables are provided in Supplementary Table S1. The parameter values are estimated using decay constants, production kinetics, cytotoxicity assays and dose–response curves, followed by fitting the equations of enzyme kinetics (e.g. Michaelis–Menten, inhibition kinetics, Lineweaver–Burke plots and multi-substrate kinetics) to the experimental data (31). The parameter values are represented in Supplementary Table S2.

*Simulation.* Model simulations are performed in MATLAB (version 2019a) as detailed in Supplementary Methods. We use Latin Hypercube Sampling (LHS) to generate uniformly distributed samples and then determine the disease outcome by numerically integrating (*simulating*) the system of equations.

### *Definition of disease outcome*

Clearance ensues when the pathogen cannot colonize the host. We assume that the host can easily clear the bacterial population of less than 100 per milliliter (equivalent to ~10 bacteria per MLN) and classify such cases as clearance. However, if the pathogen succeeds in colonizing the host, its number can increase exponentially (increasing beyond $10^5$ bacteria per milliliter of MLN) leading to active disease. Alternatively, the pathogen can maintain its number at a certain level ($10^2$–$10^5$ per gram of MLN), resulting in persistent/latent infection (4). The cases where the bacterial number is in the range $10^2$–$10^5$ per milliliter of MLN, showing a slow increase in population, are classified as L1 latency, whereas the cases with bacterial population in the range $10^2$–$10^5$ per milliliter of MLN and showing a stable population trend are classified as L2 latency. The details of disease outcome classification are also summarized in Supplementary Table S3.

### *Virtual deletion and depletion experiments*

We perform five virtual deletion and depletion experiments each, where we deplete/delete variables in combinations, namely, IFN-$\gamma^-$, (IFN-γ + IL-12)$^-$, (IFN-γ + $M_1$)$^-$, IL-12$^-$ and IL-4$^-$. We delete $M_1$ along with IFN-γ as these are typically absent in the IFN-γ knockout mice. For a virtual deletion experiment, we set a chosen combination of model variables (along with corresponding ICs) and parameters associated with its equation to zero before the introduction of the infection (31, 32), i.e. day 0. The remaining parameters are sampled from their usual ranges.

A virtual depletion experiment is performed for only those parameter samples that lead to latency (31). We start with uniformly generated parameter samples and simulate the model until the 90th day and identify the disease outcome. For samples leading to latency, we store the value of all the variables at this time point (90th day). These values serve as ICs for further simulation. Then, similar to a deletion experiment, we set the parameter values of the concerned equation(s) and the corresponding ICs (the value stored at the 90th day) to zero. After this, using the same values for the other parameters (not appearing in the depleted variable's equation) and the new ICs, we simulate the model for another 30, 110 and 210 days.

### *Global sensitivity analysis*

Since the model consists of a system of first-order ordinary differential equations that are highly non-linear, we expect the disease outcome to depend not only on the parameters, but on the ICs as well. In this sense, we expect ICs also to

and $M_{2i}$)—are considered in the model. (C) Lymphocyte interaction network. The figure represents the conversion, recruitment and proliferation kinetics of four $T_H$ lymphocytes—naive $T_H$ ($T_{HN}$), precursor ($T_{H0}$), $T_{H1}$ and $T_{H2}$ populations. (D) Cytokine production and decay kinetics. The figure represents the production of three cytokines—IL-12 ($I_{12}$), IFN-γ ($I_\gamma$) and IL-4 ($I_4$) by different cell types along with their decay parameters. (E) Bacterial kinetics. Extracellular ($B_E$) convert into intracellular on internalization with macrophages and DCs. The intracellular bacteria become extracellular when the phagocytes burst. The intracellular bacteria in $M_0$, $M_2$ and DCs are depicted as $B_{iM0}$, $B_{iM2}$, $B_{iDC}$, respectively. In all the sub-figures, the rates for different processes are depicted as alphanumeric and Greek symbols. The plus sign and minus sign signify positive and negative effects of the given variable.

Downloaded from https://academic.oup.com/intimm/article/33/5/281/6066543 by guest on 27 December 2022

be parameters of the system. However, before infection begins, the system is expected to have attained a steady state (an equilibrium point of the system in the absence of pathogens), suggesting that different ICs lead the no-pathogen model to the same steady state for a given parameter set. Therefore, we numerically investigated the no-pathogen model by generating 10 000 uniformly distributed parameter samples and 1000 uniformly distributed IC samples for each parameter sample. For a given parameter sample, it is observed that all 1000 ICs result in the same end condition and we can comfortably say that the model reaches a steady state solution. We say so as the variation in 1000 end conditions so obtained was much smaller than the variation in ICs (Supplementary Figure S1). If we fix a point in the parameter space (i.e. for a given parameter sample), ICs are not the parameters for the no-pathogen model. However, the entire parameter space cannot be replaced by a single point of the parameter space or a few representative points. This, on the one hand, establishes the necessity of the sensitivity analysis (SA) over the parameter space, and on the other hand, makes the SA over the combined IC-parameter space unnecessary. Accordingly, we have carried out SA based on samples from the parameter space only. IC values used for SA are from Supplementary Table S1.

To choose between Partial Rank Correlation Coefficient (PRCC) and extended Fourier Amplitude Sensitivity Test (eFAST) as the SA method, we examine non-monotonicity and non-linearity in the input–output relationship (33, 34) as described in Supplementary Methods. We consider $B_{total}$ at the 100th day as the model output and sampled parameters as the model input. The relationship is found to be linear and monotonic for all the sampled parameters (Supplementary Figure S2); hence, the PRCC method is chosen for further analysis.

We calculate the PRCC value (32, 34) using the rank-transformed input and output, at every 10th day starting from day 10 up to day 100 and consider only the statistically significant PRCC values ($P$-value < 0.05). This is done thrice to ensure consistency in the results. We rank the parameters based on the absolute value of their average PRCC. The scatter plots depicting the input–output relationship and the PRCC values are calculated using the MATLAB code available in the online repository of Dr D. E. Kirschner (34).

The bifurcation efficacy of the top-ranked parameters is estimated by calculating the change in disease distribution (at the 100th day) as the sampling range of the parameter is changed. The disease distribution is the percentage of each disease outcome observed in the sampled space (lowest 10% range, highest 10% range, upper-mid range and the lower-mid range) (Supplementary Methods). We calculate the root mean square difference of the two distributions (the lowest 10% to highest 10% range and the upper-mid to lower-mid range) to quantify the bifurcation efficacy of top-ranked parameters on day 100.

### *Reduced order model*

We generate a reduced order model (RoM) based on Lotka–Volterra equations for competition and prey–predator interaction (35), and the results of SA capturing the essence of full-order model. The model consists of three first-order ordinary differential equations describing the dynamics of bacteria and phagocytes (macrophages and DCs), the key players in deciding the final disease outcome. The details of the RoM construction and its parameter estimation (Supplementary Table S7) are provided in the Supplementary Methods. The RoM simulation is performed in MATLAB (version 2019a) in a manner similar to that of the full-order model.

The disease outcome is defined akin to a full-order model. The classification of outcome depends on the value obtained by the bacterial population on the 100th day. However, in RoM, we observed that the bacterial population does not show a reducing trend when the value is close to 100 per milliliter. This holds true even while we increase the simulation time to 500 days. Thus, we classify the outcome as clearance if the bacterial population is less than 10 per milliliter. If the population exceeds $10^5$ per milliliter, it is classified as active disease. If the bacterial population stays between 10 and $10^5$ bacteria per milliliter at the 100th day, then such parameter samples are classified as latency.

### *Therapeutic and prevention strategies*

To evaluate the therapeutic strategies, we start the model simulations with 10 000 samples generated from unmodified ranges of parameters. Then the simulation is interrupted at a pre-defined time point (10th, 20th and 30th day post-infection) and the values of the variables are stored. These would serve as the new ICs for resuming the simulation. The values of the chosen parameter combinations (Table 3), except for $\alpha_{23}$, are reduced or increased by 20 or 30% as indicated by their PRCC value at the 100th day. With the modified values of the chosen parameters, original values for the remaining parameters and the new ICs, the model simulation is resumed and the outcomes (at the 100th day) are noted as percentages.

To implement prevention strategies, the values of chosen parameter combinations are affected on day 0. We reduce or increase the upper and lower limits (as prescribed by the corresponding PRCC value at the 100th day) of the parameter range by 10, 20, 30 or 40% in accordance with the vaccination results (36–39). With the remaining parameters sampled from their original ranges, we generate 10 000 samples and determine the disease distribution. The effectiveness of a prevention strategy is judged by comparing the percentage of clearance cases with and without implementation.

## Results

### *Baseline simulation and biological insights from model simulation*

The baseline simulation is performed using the arithmetic mean of the range of each parameter of the model. The outcome for baseline simulation is presented in Supplementary Figure S3 as a plot depicting the time history of the total bacterial load ($B_{total} = B_E + B_{iM0} + B_{iM2} + B_{iDC}$).

The interaction between the host and *Salmonella* is expected to lead to clearance, active disease or latency. Our model simulation predicts 50.38% clearance, 13.8% active disease and 35.82% latency (L1: 11.64% and L2: 24.18%)

Downloaded from https://academic.oup.com/intimm/article/33/5/281/6066543 by guest on 27 December 2022

cases for 10000 uniformly distributed parameter samples. These values are in line with the reported risks for each outcome (34, 40). The representative plots for each disease outcome for the bacterial population dynamics are provided in Fig. 2. In the following sections, we discuss the bacterial, immune cell and cytokine dynamics for the disease outcomes, relating it with the observations in the murine typhoid model.

### *Bacterial, cellular and cytokine dynamics*

*Bacterial dynamics.* For clearance cases, bacterial populations increase in time up to 10 days (2 days in Fig. 2A) and then start decreasing (Fig. 2A). For active disease, the bacterial populations increase linearly on the logarithmic scale (Fig. 2B). The model predicts the onset of active disease (where $B_{total} > 10^5$ per milliliter) as early as the 12th day (20th day in Fig. 2B). The average time to the onset is 41 days with standard deviation of 18.95 days. At a later time point (35th day in Fig. 2B) after the onset, the extracellular bacterial population grows with a much larger exponent (attaining population size > $10^{10}$ per milliliter). This happens when the intracellular bacterial population exceeds the maximum carrying capacity of the infected macrophages. This time point corresponds to the bursting of infected macrophages (Fig. 3C). It is found that the bursting and release of intracellular bacteria takes place within 64 days (mean: ~24 ± 13 days) of the commencement of active disease (where $B_{total} = 10^5$ per milliliter). It was found that just before the demise of the infected mice, the bacterial load in the blood attains a value closer to $10^{10}$ per milliliter (5). So soon after this point, we expect the mice would succumb to the infection. For latency cases, we observe a lag (40 days, Fig. 2C and 12 days, Fig. 2D) before the bacterial number starts increasing and most of the time stabilizing at a value in the range $10^2$–$10^5$ per milliliter. The lag period is ~41 ± 15 and 30 ± 12 days for L1- and L2-type latency cases, respectively, and can be as small as 4–5 days. Such a lag is also observed for the active disease cases. Similar to the reported chronic infection conditions (4, 13), our model predicts more than 80% of the total bacteria being intracellular on the 100th day during latency ($B_i >> B_E$, Fig. 2C and D). Moreover, it is also reported that 82% of *Salmonella* persists within macrophages in chronically infected mice, which is in good agreement with the model prediction [more than 96% are within macrophages (4, 13)].

*Cellular dynamics.* During clearance and latency, uninfected macrophages and DCs show some deviation (a maximum of 8-fold increase) from the initial value (Fig. 3A and B). For active disease, uninfected macrophages and DCs decrease substantially while becoming infected (Fig. 3A and B). During the initial period, the infected macrophage and DC populations increase exponentially and later attain equilibrium at a time point (52nd day Fig. 3C and 42nd day, Fig. 3D) in a regime with extracellular bacteria outnumbering the intracellular bacteria (beyond 35th day, Fig. 2B). Before attaining equilibrium, the infected macrophage population decreases moderately (from 35th to 52nd day, Fig. 3C), owing to the bacteria-induced bursting of these cells. This coincides with the time point where the extracellular bacterial population starts growing with a larger exponent (35th day, Fig. 2B). The bursting of macrophages can be deemed as bacteria-induced tissue damage. During active disease, the infected macrophage number is $10^3$–$10^5$ times higher than that during latency.

For latency cases, the model predicts significant alterations in the ratios of anti-inflammatory and pro-inflammatory macrophages ($M_2/M_1$), and $T_{H2}/T_{H1}$ ratios as well. In many of the latency cases, we observe that proportions of anti-inflammatory $M_2$ macrophages (Fig. 3E) and $T_{H2}$ cells (Fig. 3F) increase with time, indicating a $T_{H2}$ bias. We retrieve the population count of $T_{H1}$, $T_{H2}$, $M_2$ and $M_1$ for all latency cases (35.82% of total) at early (5th day) and late (90th day) time points. We do the same for all active disease cases (13.8% of total) at the same early time point as latency and late time point based on 5 days after $B_{total} = 10^5$ per milliliter. We observe that the cases with $M_2 > M_1$ increase from 0% (early time point) to 60.2% (late time point) for L1 latency and 0.08 to 45.8% for L2 latency (Fig. 3G) cases. Similarly, the cases with $T_{H2} > T_{H1}$ increase from 6 to 89.4% for L1 type and 5.6 to 88.6% for L2 type (Fig. 3G). For active disease, there is a small increase in these values. The cases with $M_2 > M_1$ increase from 0 to 7.8%, while those with $T_{H2} > T_{H1}$ increase from 8 to 39.6% (Fig. 3G). These results are similar to the reported $T_{H2}$ bias and $T_{H1}$ bias in the mice with persistent and acute *Salmonella* infection, respectively (27).

*Cytokine dynamics.* The IFN-γ cytokine peaks ($10^3$–$10^4$ pg $ml^{-1}$) within the first 2–3 days for all four outcomes (Fig. 4), signifying the initiation of the infection (27). It is known that within 5 days of infection in susceptible mice (active disease), the IFN-γ increases by 500- to 1000-fold (41, 42). Correspondingly, our model predicts an up to 1000-fold increase in IFN-γ levels (>$10^3$ pg $ml^{-1}$) during active disease, and this level is sustained throughout (Fig. 4B). Studies in chronically infected (latency) mice suggest a 100- to 1000-fold increase in the IFN-γ within first 5–10 days (41, 43). However, at later time points, its concentration decreases by ~10-fold and remains stable for up to at least 30–40 days post-infection (8, 41). In line with this and other reports (18, 44, 45), our model predicts higher IFN-γ (>350 pg $ml^{-1}$ in more than 80% of cases) during latency (Fig. 4C and D). This increase is irrespective of the low $T_{H1}$ response (Fig. 3F and G). Higher IFN-γ levels promote the generation of pro-inflammatory anti-bacterial $M_1$ macrophages, controlling the bacterial number. However, this may potentiate tissue damage. For clearance cases, there is an initial spike in IFN-γ concentration, indicating hosts' response to bacterial invasion. Following this, the IFN-γ concentration reduces, stabilizing at a value closer to the baseline (Fig. 4A).

For most of the latency cases, our model estimates an initial increase in IL-12 level (4- to 120-fold), followed by a drop (Fig. 4C and D). Subsequent to this, the levels increase, stabilizing at a value up to 4- to 200-fold higher than the baseline value (Fig. 4C and D). Additionally, in many of the latency cases, IL-4 attains a higher value (Fig. 4C and D), probably linking to a higher $T_{H2}$ response, while for others, the value is close to or less than the baseline. These predicted IL-12 and IL-4 kinetics are in accordance with the reported kinetics of IL-12/IL-12p70 (a heterodimer produced by macrophages and DCs) and IL-4 during chronic *Salmonella* infection (8, 46). *In vivo* studies suggest that the chronically infected mice can

Downloaded from https://academic.oup.com/intimm/article/33/5/281/6066543 by guest on 27 December 2022

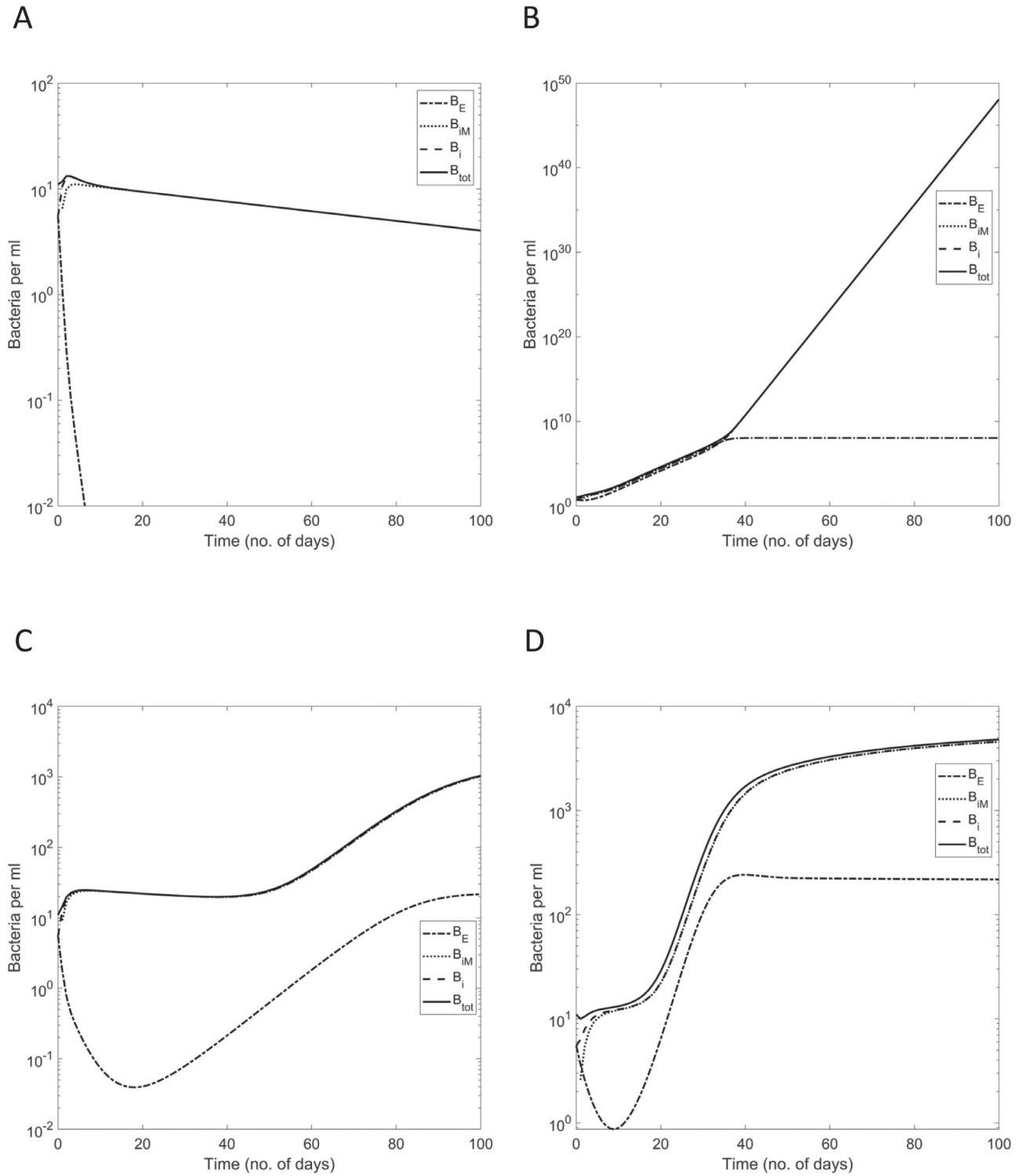


**Fig. 2.** Bacterial population dynamics for different disease outcomes. Representative plots obtained after 100 days of model simulation depicting four types of bacterial population trajectories are depicted. Time history of bacterial populations for clearance (A), active disease (B), L1-type latency (C) and L2-type latency (D) was obtained after model simulation in MATLAB. The y-axis represents the bacterial population per milliliter of MLN and the scales are different for each sub-part as the bacterial numbers in each case are of different magnitudes.

show either increased or decreased IL-4 levels (45). We observe a similar trend with our model simulations. As expected and depicted in Fig. 4, the IL-12 concentration is generally maintained at a lower value (<200 pg ml$^{-1}$) during clearance and at a higher value during active disease (>$10^3$ pg ml$^{-1}$) (47, 48). As reported in murine typhoidal studies (8, 45, 46),

Downloaded from https://academic.oup.com/intimm/article/33/5/281/6066543 by guest on 27 December 2022

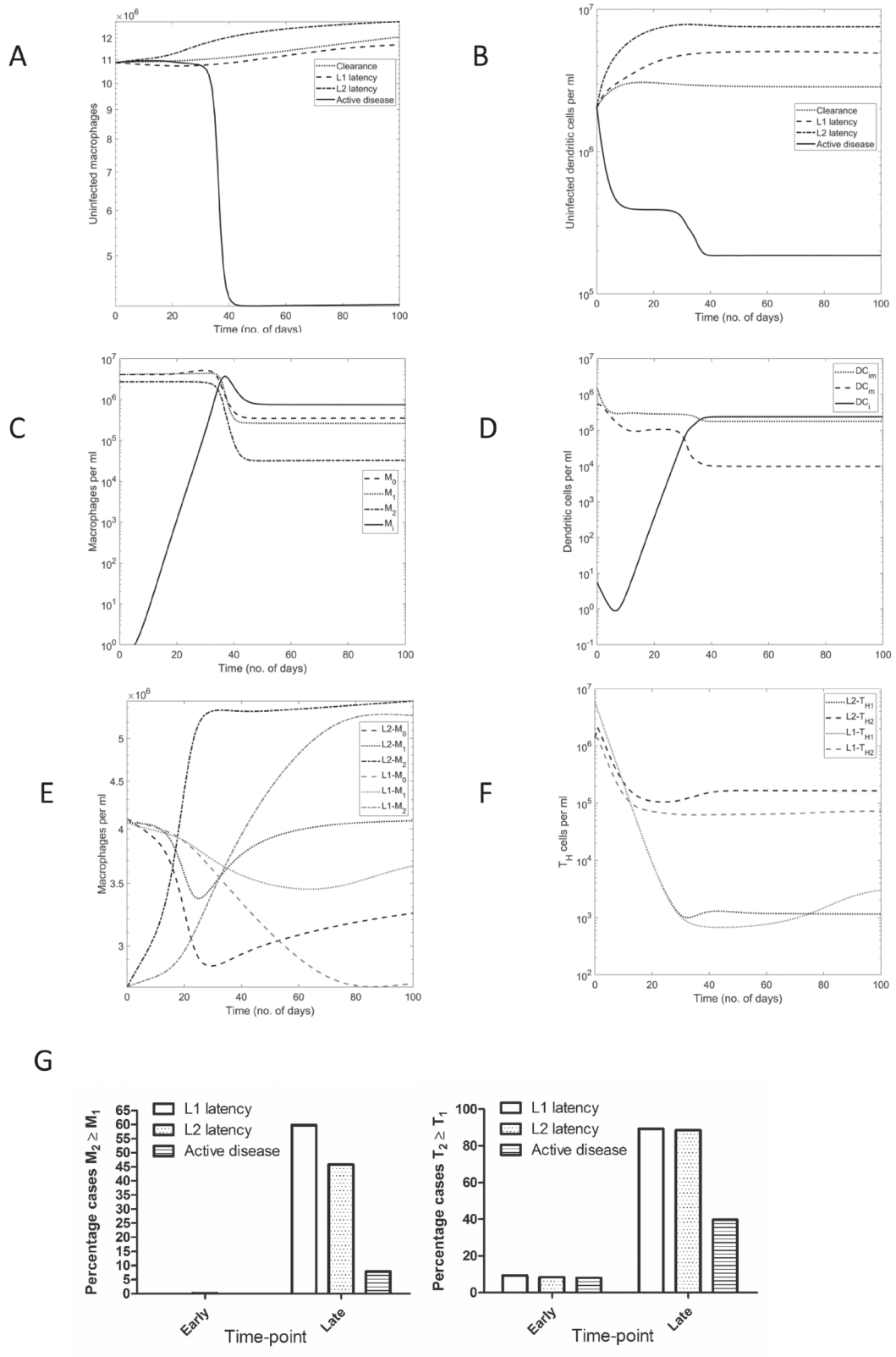


**Fig. 3.** Immune cell dynamics operational during different disease outcomes. Plots for different immune cells were obtained after simulating the model in MATLAB for 100 days. (A, B) Representative plots depicting the time history of uninfected macrophages (A) and dendritic cells (B) during the four disease conditions. (C, D) Plots representing the different macrophage and DC populations during active disease. The decrease in uninfected macrophages/DCs coincides with the increase in infected macrophages/DCs. (E, F) Plots representing the dynamics of different types of macrophages and $T_H$ cells during latency. There is an increase in the proportion of $M_2$ macrophages (E) and $T_{H2}$ (F) cells in both L1- and L2-type latency cases. (G) The statistics of $M_2/M_1$ and $T_{H2}/T_{H1}$ ratio during the four disease outcomes at early (5th day) and late (90th day: latency and 5th day after the onset of active disease: active disease) time point. Y-axis for all the graphs except in (G) represents cells per milliliter of MLN.

Downloaded from https://academic.oup.com/intimm/article/33/5/281/6066543 by guest on 27 December 2022

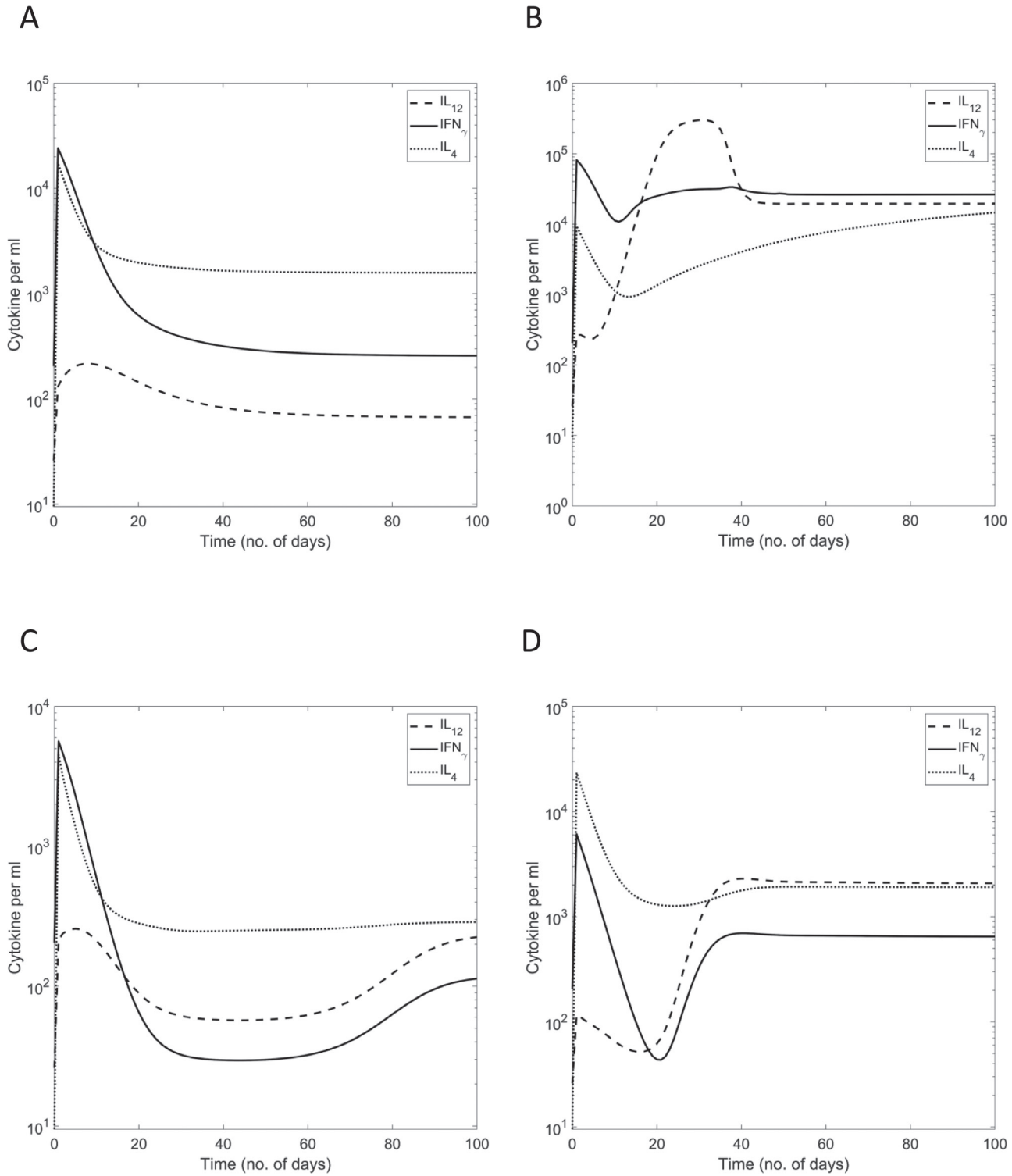


**Fig. 4.** Cytokine dynamics operational during different disease outcomes. Plots for different immune cells were obtained after simulating the model in MATLAB for 100 days. Representative plots of the time history of cytokines during clearance (A), active disease (B), L1 latency (C) and L2 latency (D) are depicted. *Y*-axis for all the graphs represents cytokines per milliliter of MLN.

the IL-4 concentration varies significantly within all disease outcomes, suggesting that the IL-4 (or $T_{H1}/T_{H2}$ balance) alone may not have a major role in deciding the disease outcome. In addition, high IL-4 during active disease may indicate an anti-inflammatory response important for neutralizing the tissue damage.

Downloaded from https://academic.oup.com/intimm/article/33/5/281/6066543 by guest on 27 December 2022

*Relative role of cytokines through virtual deletion and depletion experiments*

*Virtual deletion.* Studies based on knockout mice have revealed the importance of different immune system components, such as IFN-γ, IL-12 and iNOS in defining the course of *Salmonella* infection (13, 18, 43, 49, 50). However, the knockout mutation of these components might alter non-target pathways or dysregulate the immune response, thus hampering the precise analysis of the exclusive effect of the mutation. To understand the specific roles of IFN-γ, IL-12 and IL-4, we simulate the model for 100 days by virtually deleting a chosen combination of these model variables.

The percentage of active disease cases increases by 4- to 5.5-fold in all deletion experiments except IL-4-deletion (Table 1). On deletion of pro-inflammatory cytokines, the system progresses to active disease (10 days, Supplementary Figure S4A) and latency at a faster rate. The average time required to attain active disease is 26 ± 15 days on IFN-γ deletion and the average lag period for L1 and L2 latencies is ~28 ± 10 and 26 ± 6 days, respectively. These results corroborate with the results from IFN-γ- and IL-12-deficient mice/human patients, showing increased susceptibility to *Salmonella* infection (18, 43, 50). The entire system does not progress to active disease on IL-12 or IFN-γ deletion, indicating that inflammation is essential but not sufficient for controlling the infection. Our model predicts fewer active disease cases with IL-12 deletion than that with IFN-γ deletion (Table 1). We observe that IFN-γ + IL-12 deletion gives almost the same proportions of various disease outcomes, while IFN-γ + $M_1$ gives a higher proportion of active disease when compared with IFN-γ deletion (Table 1). Many parameter samples that result in clearance/latency under normal circumstances induce active disease in the absence of IFN-γ (Supplementary Figure S4B and C). This could be due to the reduction of $M_1$ macrophages and $DC_m$, which are potent bacterial killers (Supplementary Figure S4D and E). Consequently, there is also an increase in the number of bacteria conducive $M_2$ macrophages. Similar to the reported lymph node infiltration by mononuclear cells in the absence of IL-12 (hence IFN-γ), our model predicts an increase in total macrophage number in IFN-γ deletion experiments (Fig. 5A) along with an increase in the proportion of $T_{H2}$ cells for active disease cases (Fig. 5B).

As depicted in Table 1, the results of the IL-4 deletion experiment reveal a 25.63% increase in the clearance cases with a subsequent decrease in both active disease (decrease by 3.74%) and latency cases (decrease by 21.89%). Deletion of IL-4 increases the lag period while decreasing the severity of the disease (Supplementary Figure S5A) and some of the expected latency cases progress to clearance (Supplementary Figure S5C). The model indicates consistent $T_{H1}$ bias (Fig. 5B and Supplementary Figure S5F), typically expecting to reduce the active disease and latency percentages, significantly higher than the above-mentioned values. Deletion of IL-4 increases the proportion of $M_1$ macrophages (Supplementary Figure S5E) but not the concentration of IFN-γ and IL-12 (Supplementary Figure S5B and D).

*Virtual depletion.* Cytokine neutralization experiments in mice and anti-inflammatory treatment in humans have demonstrated that depletion of IFN-γ reactivates persistent *Salmonella* infection. To mimic the neutralization experiment, we perform five virtual depletion experiments in combinations similar to that of deletion. The results indicate reactivation (Supplementary Figure S6A) of most latency cases within 30 days of depletion (Table 1) for all combinations except IL-4 depletion. The system takes 60–150 days (60 days: IFN-γ + M1; 100 days: IFN-γ; and 150 days: IL-12 depletion) to achieve complete reactivation, implying a slow deterioration of the immune system in some cases (<10%). The percent reactivation is marginally higher with IFN-γ + $M_1$ and lower with IL-12 depletion compared with the reactivation with IFN-γ depletion (Table 1). We attribute the reactivation to the absence/decrease of $M_1$ macrophages and $DC_m$ having high anti-bacterial potential (Supplementary Figure S6B and C). Concomitantly, the IFN-γ and IL-12 depletion experiments predict an increase in the proportion of $T_{H2}$ cells (Fig. 5D), further escalating the reactivation of latency cases. As expected, the model predicts an increase in total macrophage number in IFN-γ depletion experiments, followed by a drop (day 113, Fig. 5C) which is indicative of macrophage bursting (a typical characteristic of active disease).

On depleting IL-4 after latency is achieved, the model predicts recovery of some (1%) latency cases (Table 1). There is a conversion of almost all L1 latency cases to L2 latency (Table 1 and Supplementary Figure S6D), indicating attenuation of disease symptoms. We relate this to the increase in the $T_{H1}$ response (Fig. 5D), resulting in overall reduction of bacterial growth.

*Reactivation and re-infection.* When we simulate the model without any deletion/depletion over a longer period

**Table 1.** Percentage of disease outcomes on virtual deletion and depletion of model variables

| Disease | No deletion/depletion | IFN-γ | IFN-γ + IL-12 | IFN-γ + $M_1$ | IL-12 | IL-4 |
|---|---|---|---|---|---|---|
| Deletion | | | | | | |
| Clearance | 50.38 | 24.02 | 24.06 | 17.59 | 39.63 | 76.01 |
| Active disease | 13.8 | 64.01 | 63.21 | 74.68 | 53.3 | 10.06 |
| L1 latency | 11.64 | 1.63 | 2.15 | 6.26 | 6.68 | 7.77 |
| L2 latency | 24.18 | 10.34 | 10.58 | 1.47 | 0.39 | 6.16 |
| Depletion (of only latency cases) | | | | | | |
| Clearance | 0 | 0 | 0 | 0 | 0 | 0.7732 |
| Active disease | 1.76 | 95.0678 | 96.0174 | 97.709 | 90.8935 | 0.2864 |
| L1 latency | 13.9 | 4.9034 | 3.9826 | 2.291 | 9.1065 | 0.4868 |
| L2 latency | 87.86 | 0.0288 | 0 | 0 | 0 | 98.4536 |

Downloaded from https://academic.oup.com/intimm/article/33/5/281/6066543 by guest on 27 December 2022

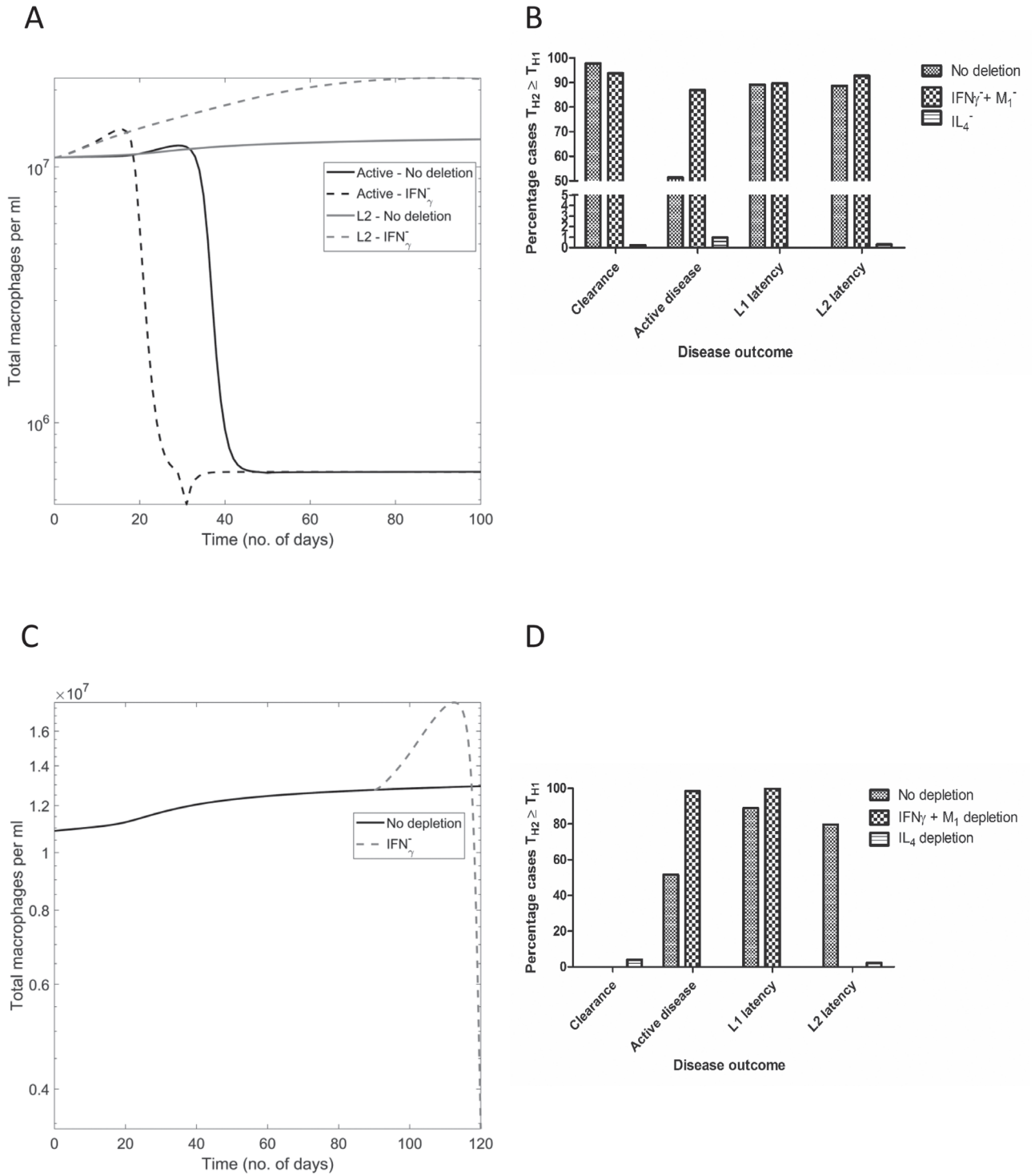


**Fig. 5.** Macrophage and lymphocyte dynamics during virtual deletion and depletion. Representative plots depicting the time history of total macrophages on (A) deleting and (C) depleting IFN-γ. Y-axis for the graphs represents total macrophage per milliliter of MLN. The statistics of $T_{H2}/T_{H1}$ ratio during on virtually deleting (B) and depleting (D) IFN-γ and IL-4 for four disease outcomes. The plots in (D) are for the results obtained after 30 days of depletion. On depletion of IFN-γ and $M_1$ macrophages, there were no cases of L2 latency, hence, in the graph, there is no bar for of IFNγ and $M_1$ depletion.

(300 days), we obtain two atypical cases. We define those as reactivation and re-infection/recurrence on the basis of transition of an outcome from the 100th to the 300th day. Reactivation occurs when the model transits from latency to active disease (Fig. 6A), and re-infection of the clearance case ensues when the bacterial population gradually

Downloaded from https://academic.oup.com/intimm/article/33/5/281/6066543 by guest on 27 December 2022

increases beyond $10^2$ per milliliter (Fig. 6B). We notice that 1–1.7% of total latency cases (~0.4–0.6% of the total cases) are reactivated within 300 days of simulation, and 5% of clearance cases are re-infected progressing to latency. These values are close to the biologically observed rates of reactivation and relapse (27, 51). The cases with reactivation show a gradual increase in IL-12, IL-4, $M_2$ and $T_{H2}$ levels (Supplementary Figure S7A, C and E) favoring increased bacterial replication. The bacterial number increases rapidly in the regime where IL-4 >> IFN-γ, $M_2$ >> $M_1$ and $T_{H2}$ >> $T_{H1}$ (Supplementary Figure S7). A higher value of both IL-4 (>$10^3$ pg ml$^{-1}$) and IFN-γ (>$10^4$ pg ml$^{-1}$) is indicative of tissue damage. During re-infection, the cytokines are close to the baseline level with a slight perturbation when the bacterial number starts increasing (Supplementary Figure S7B), and the proportion of $M_2$ macrophages and $T_{H2}$ cells is high. We propose that the re-infection event is a result of reseeding or fresh infection as indicated by the slow increase in $B_E$ (Fig. 6B).

### *Global SA and insights into factors governing infection outcomes*

The set of parameters crucial in deciding the disease outcome are identified by generating a sensitivity index called PRCC. Then, we rank the parameters from the most influential to the least influential at every 10th day starting from day 10 up to day 100 (Supplementary Table S4). The most influential (top-ranked) parameters are the potential bifurcation parameters capable of significantly changing the total bacterial load (at the 100th day) and thereby changing the disease outcome. Further, we test bifurcation efficacy of the top-ranked parameters by calculating the change in disease distribution as the sampling range of the parameter is changed. The results of bifurcation efficacy are presented in Fig. 7, confirming the correlation between the ranking and its bifurcation potential.

The results of global SA reveal the important parameters affecting the total bacterial number. The efficacy of 15 top-ranked parameters (at the 100th day) in influencing the model dynamics is analyzed. We categorize these parameters into two types relating to the bacterial attributes and host immune mechanisms (Table 2). It is observed that the number of bacterial attributes influencing the disease trajectories increases with the progression in disease (three attributes on day 10 to six attributes on day 100; Supplementary Table S4), highlighting the significance of bacterial potential in the later phase of infection.

The key mechanisms leading to different disease outcomes are presented in Table 2. The role of activated phagocytes (macrophages and DCs) is accentuated, implying the significance of stronger innate immune response in controlling the disease. Most (12 out of 15) of the top-ranked parameters (at the 100th day) are predicted to have a role throughout the course of disease (highlighted in bold in Table 2), while a few parameters are important in the initial stages and some during the later stages. For example, $\alpha_8$, $c_8$ and $c_{17}$ are highlighted only in the later stages of the disease progression, while $\alpha_{26}$, $\alpha_{35}$ and $c_{10}$ are important during early stages.

### *Reduced order model*

The results of SA highlight the importance of macrophages and DCs in governing the final disease outcome. Thus, we

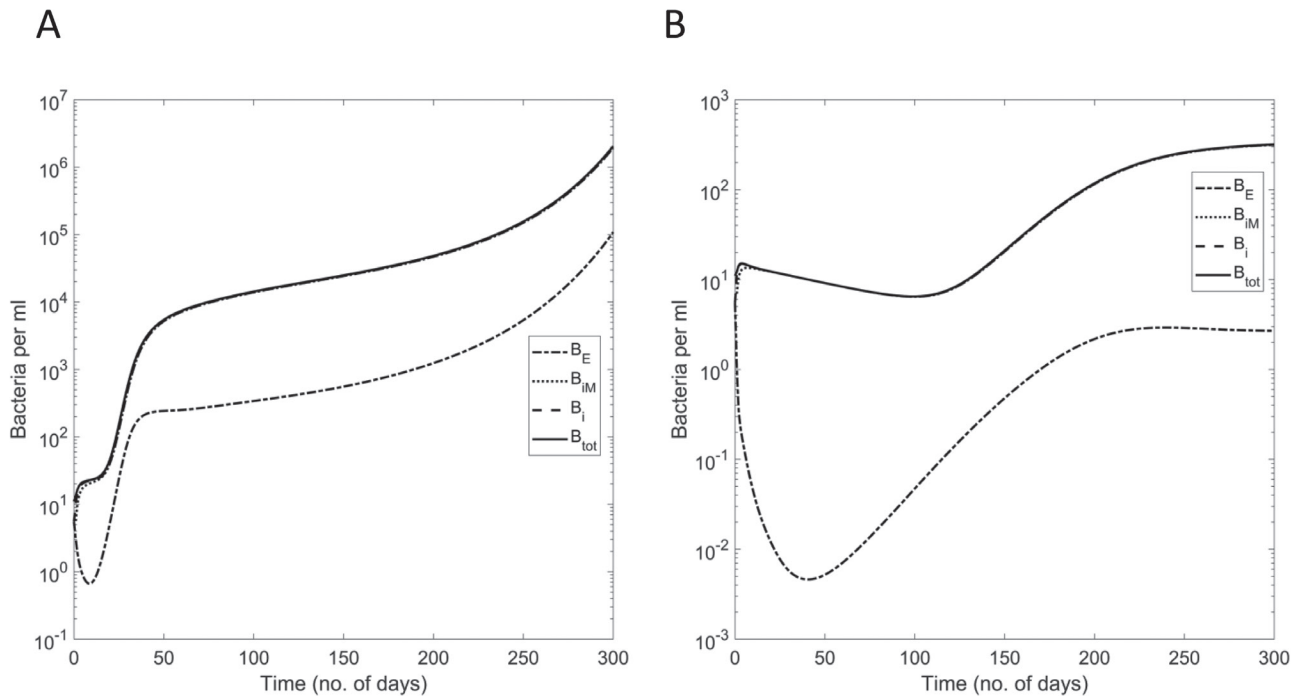


**Fig. 6.** Bacterial population dynamics during reactivation (A) and re-infection (B). Representative plots obtained after 300 days of model simulation depicting four types of bacterial population trajectories for each case. Y-axis for all the graphs represents bacteria per milliliter of MLN.

Downloaded from https://academic.oup.com/intimm/article/33/5/281/6066543 by guest on 27 December 2022

generated an RoM consisting of three variables, macrophages, DCs and bacteria on the basis of competitive and prey–predator Lotka–Volterra equations (35). This low-dimensional dynamical system approximates the basic dynamics of the full-order model, reinforcing the results of SA. The top 15 parameters identified through SA are represented (directly or indirectly) in the RoM. For example, $\alpha_{23}$, $s_1$, $\mu_1$, $\alpha_{12}$, $\alpha_{14}$, $\delta$ and $\alpha_{24}$ are considered in their original form, at times with minor modifications. While others are considered while calculating the values of modified parameters such as $\alpha_8$ and $c_8$ (considered in the estimation of $\gamma$), and $N_c$ (considered while estimating $\alpha_{13}$ and $\alpha_{24}$). Furthermore, $\mu_{16}$, $c_3$ and $c_{17}$ essentially influence the proportion of $DC_m$ and $M_1$. This effect is captured while calculating $\widehat{\gamma}$ and $\widehat{\mu_4}$, where we consider the increase in the proportion of $DC_m$ (52) and $M_1$ (18) during *Salmonella* infection.

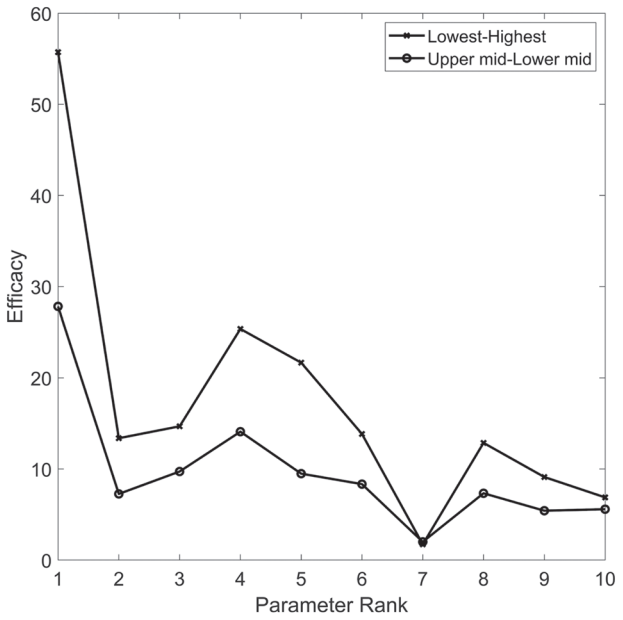


**Fig. 7.** Efficacy (bifurcation potential) of the top 10 parameters (at the 100th day) in changing the disease outcome. The parameters ranked higher by sensitivity analysis are expected to have higher efficacy. This correlation between the bifurcation potential and the parameter rank is confirmed by the decreasing trend of the efficacy.

The RoM simulations predict 60.04% clearance, 14.99% active disease and 24.97% latency cases (Fig. 8A). This shows a 9.66% increase in clearance, 1.19% increase in active disease and 10.85% decrease in latency cases when compared to the predictions of the full-order model. Similar to the active disease trajectories of the full-order model, the bacterial number increases exponentially but stabilizes at $10^{10}$ per milliliter (carrying capacity for bacterial population). However, the bacterial population trends differ for latency and clearance cases. As opposed to the full-order model, we do not observe a lag period for bacterial trajectories during latency (Fig. 8D) and a initial spike in bacterial population during the clearance cases (Fig. 8C).

### *Predictions of therapeutic and prevention strategies*

*Therapeutic strategies.* Considering the lag of 4–5 days in detecting *Salmonella* in the MLN of infected mice and 6–30 days of incubation period (53, 54) of typhoid, therapeutic strategies are implemented at time points on the 10th, 20th or 30th days of simulation. Typically, antibiotic therapy is an effective treatment for typhoid fever, and hence we modeled this effect as one of the therapeutic strategies. Administration of antibiotics is expected to significantly reduce the growth

**Table 2.** First 15 top-ranked significant parameters and the process they control along with possible intervention strategy

| Parameter (attribute) | PRCC value | Process controlled (key mechanism) | Possible intervention |
|---|---|---|---|
| **$\alpha_{23}$ (bacterial)** | **0.8732** | **Virulence potential** | **Antibiotics can decrease the value** |
| **$\alpha_{24}$ (bacterial)** | **0.2204** | **Virulence potential** | **Antibiotics can decrease the value** |
| **$N_c$ (bacterial/host)** | **–0.3479** | **Virulence potential. Macrophage's bacterial holding potential** | |
| $\alpha_8$ (bacterial/host) | –0.2101 | Virulence potential. Macrophage's phagocytic potential | Increase through vaccination |
| $c_8$ (bacterial/host) | 0.1897 | Virulence potential. Macrophage's phagocytic potential | Decrease through vaccination |
| $c_{17}$ (bacterial/host) | 0.1362 | Virulence potential. Macrophage's induction potential | |
| **γ (host)** | **–0.4310** | **$M_1$ macrophage's anti-microbial potential** | **IFN-γ therapy to stimulate $M_1$ production** |
| **$\mu_{16}$ (host)** | **0.3678** | **Controls phagocyte's anti-microbial potential** | **Recombinant IFN-γ with increased half-life** |
| **$s_1$ (host)** | **–0.3313** | **DC recruitment/natural turn-over** | **$CCR7_+$ DC adoptive transfer** |
| **$\mu_2$ (host)** | **0.3205** | **$DC_m$ natural turn-over** | |
| **$\mu_1$ (host)** | **0.2064** | **$DC_{im}$ natural turn-over** | |
| **δ (host)** | **–0.1481** | **DC's anti-microbial potential** | **Recombinant IFN-γ with increased half-life/activated $CCR7_+$ DC adoptive transfer** |
| **$c_3$ (host)** | **0.2048** | **Controls DC's anti-microbial potential** | **Indirectly through increasing IFN-γ supply** |
| **$\alpha_{12}$ (host)** | **–0.1754** | **Cytolytic potential of effector cells** | **Increase through vaccination** |
| **$\alpha_{14}$ (host)** | **–0.0938** | **Cytolytic potential of effector cells** | **Increase through vaccination** |

Twelve of 15 of the top-ranked parameters (at the 100th day) are predicted to have a role throughout the course of disease (highlighted in bold).

Downloaded from https://academic.oup.com/intimm/article/33/5/281/6066543 by guest on 27 December 2022

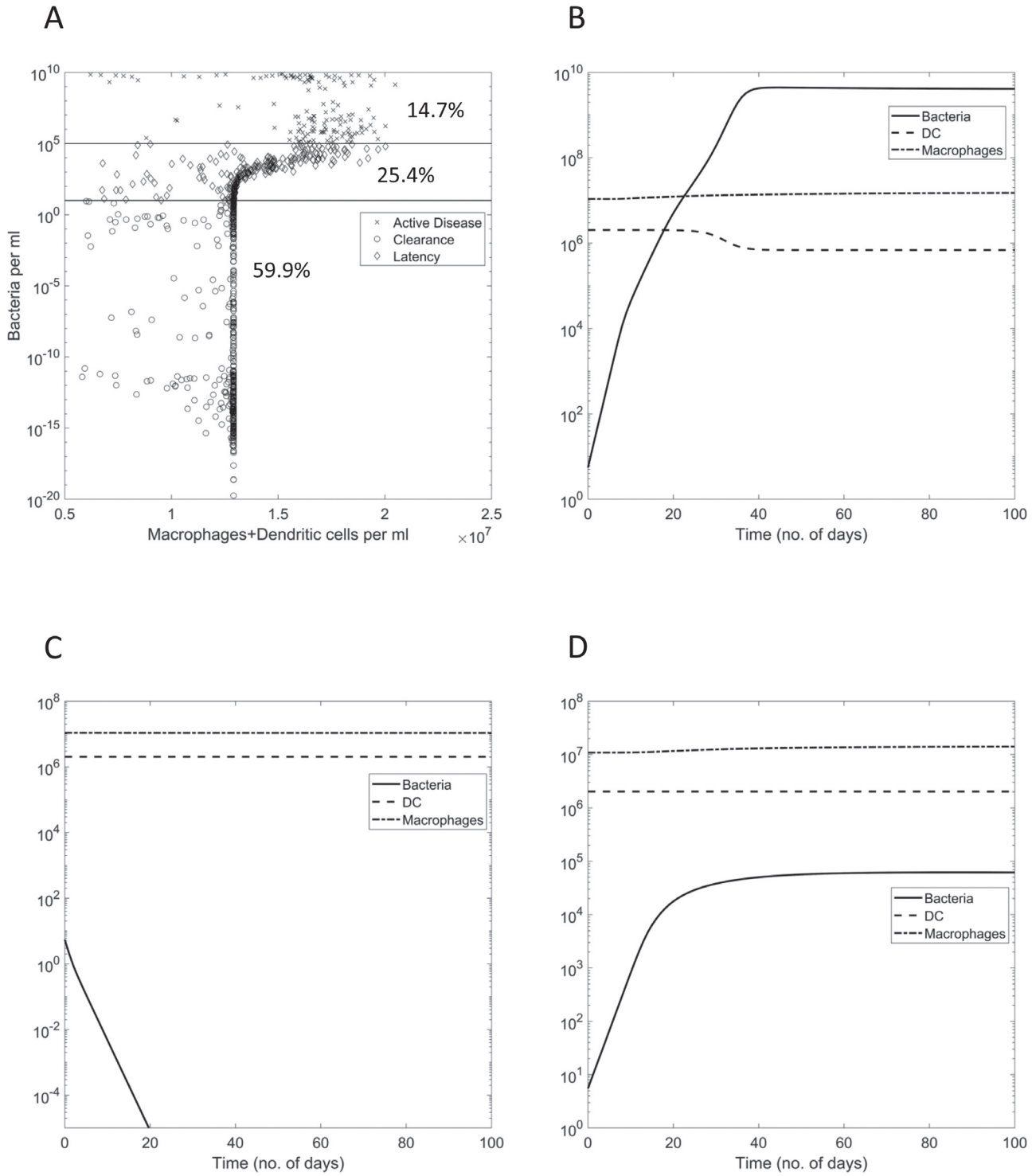


**Fig. 8.** (A) Distribution of the three disease outcomes on macrophage/DC versus bacteria population plot derived after RoM simulation. Increasing bacterial population induces an immune response which can be seen from increasing macrophage and DC population. Time history of bacterial populations for active disease (B), clearance (C) and latency (D) was obtained after RoM simulation in MATLAB. The Y-axis represents the cell population per milliliter of MLN and the scales are different for each plot as the bacterial numbers in each case are of different magnitude. For active disease (B), the bacteria can be seen saturating close to maximum carrying capacity. For clearance (C), the bacteria are cleared early. For latency (D), the bacteria saturate at a value at least five orders lower than the maximum carrying capacity.

rate of bacteria. To implement this effect, we reduce the upper and lower limits (by 50, 66 and 80%) of growth rate of extracellular ($\alpha_{23}$) and intracellular ($\alpha_{24}$, and $\alpha_{26}$, with 30% shift) bacteria at the desired time points and note the percent outcomes. In accordance with the results of SA, a significant reduction in active disease cases was observed by adjusting

Downloaded from https://academic.oup.com/intimm/article/33/5/281/6066543 by guest on 27 December 2022

**Table 3.** Therapeutic and prevention strategies

| Therapeutic strategies implemented at the 10th day with 30% shift in parameter range | | | | | Prevention imposed with 40% effect on different parameters | | | | |
|---|---|---|---|---|---|---|---|---|---|
| Combination | C | AD | L1 | L2 | Combination | C | AD | L1 | L2 |
| Untreated | 50.45 | 13.77 | 12.17 | 23.61 | Unvaccinated | 50.45 | 13.77 | 12.17 | 23.61 |
| Antibiotics with other therapeutic strategies | | | | | Vaccination related | | | | |
| 50% reduction in $\alpha_{23}$ | 89.97 | 0.26 | 2.35 | 7.42 | $\alpha_{23}$ | 85.88 | 0.99 | 7.34 | 5.79 |
| 50% reduction in $\alpha_{23}$, $\alpha_{24}$ and $\alpha_{26}$ | 90.59 | 0.25 | 2.23 | 6.93 | $\alpha_{23} + \mu_{16}$ | 89.37 | 0.66 | 5.72 | 4.25 |
| 80% reduction in $\alpha_{23}$ | 96.33 | 0 | 0 | 3.67 | $\alpha_{23} + \alpha_8 + c_8$ | 97.7 | 0.07 | 1.65 | 0.58 |
| Alternative therapeutic strategies | | | | | $\alpha_{23} + \alpha_8 + c_8 + \alpha_{35}$ | 97.83 | 0.05 | 1.6 | 0.49 |
| $\mu_{16}$ (range change) + $\gamma + c_3 + s_1 + \mu_1 + \mu_2$ | 90.07 | 1.09 | 1.44 | 7.4 | Vaccination related + new strategies | | | | |
| $\mu_{16}$ (range change)+ $\gamma + c_3 + \alpha_8 + c_8 + s_1$ | 90.52 | 1.11 | 2.4 | 5.97 | $\alpha_{23} + \alpha_8 + c_8 + \gamma$ | 98.65 | 0.01 | 0.93 | 0.41 |
| $\alpha_8 + c_8 + N_c$ | 81.03 | 3.26 | 7.16 | 8.55 | $\alpha_{23} + \alpha_8 + c_8 + \gamma + \mu_{16}$ | 99.07 | 0.01 | 0.69 | 0.23 |
| $\alpha_8 + c_8 + N_c + \mu_2$ | 82.4 | 2.12 | 5.15 | 9.97 | $\alpha_{23} + \alpha_8 + c_8 + N_c$ | 99.47 | 0 | 0.40 | 0.13 |
| $\mu_{16}$ (range change) + $\alpha_8 + c_8 + N_c$ | 89.56 | 1.36 | 3.23 | 5.85 | $\alpha_{23} + \mu_2$ | 89.69 | 0.38 | 4.98 | 4.95 |

the value of only $\alpha_{23}$, while a combination with $\alpha_{24}$ and $\alpha_{26}$ did not improve the treatment efficacy (Table 3). The maximum efficacy is achieved by implementing the intervention on the 10th day with 80% reduction in $\alpha_{23}$, which substantially decreases the incidences of active disease and latency (Supplementary Table S5). In line with the clinical patient antibiotic treatment data, the model predicts ~96% clearance and 2–10% of latency cases after the implementation of different treatment strategies (27, 54). We implement combinatorial therapies to improve therapeutic efficiency through a decrease in the latency cases. The incidences of latency are reduced by affecting the following parameters, $\mu_{16}$, $N_c$, $\gamma$ and a combination of $\alpha_8$ and $c_8$ along with $\alpha_{23}$ (Supplementary Table S5). During latency, the bacteria are majorly within $M_0$ and $M_2$ macrophages. Consequently, critically decreasing the $M_0$ and $M_2$ macrophages (by increasing the death rate by 500–1000 times) resulted in 100% clearance cases.

Emergence of antibiotic-resistant strains necessitates alternative therapeutic strategies (54, 55). On the basis of the results of SA, we incorporate new strategies by affecting (i) the phagocytic and bacterial killing potential of macrophages; (ii) DC recruitment, activation and natural turn-over; (iii) cytolytic potential of effector cells; and (iv) IFN-γ half-life (1.84–4/day) in combinations listed in Table 3 and Supplementary Table S5. Affecting $\mu_{16}$, $\gamma$, $c_3$, $\alpha_8$, $c_8$ and $s_1$ simultaneously by 30% on the 10th day gives best efficiency, resulting in 90.52% clearance cases (Table 3).

*Prevention strategies.* Vaccination acts as a practical public health tool for preventing the occurrence of disease (36–38, 56, 57). We capture the vaccination effect by affecting the phagocytosis, bacterial killing and cytokine production by immune cells through appropriate changes in the corresponding parameters (36–38, 57). The percentages of clearance cases after suitably modifying the ranges of parameters mimicking the vaccination effect are listed in Table 3. Maximum effect (~98% clearance cases) is obtained when the parameters—$\alpha_{23}$, $\alpha_8$, $c_8$ and $\alpha_{35}$—are simultaneously modified by 40%, with $\alpha_{23}$ being the most influential parameter and $\mu_{16}$ and $\alpha_{35}$ being the least influential (Supplementary Table S6). We also impose different prevention strategies to improve the vaccination efficacy. We suitably modify the ranges of selected parameters, especially those highlighted by the SA, in different combinations. The efficacy of vaccination increased by altering $N_c$ and $\gamma$ along with the parameters mimicking vaccination (Table 3). Maximum prevention is achieved by altering the range of $\alpha_{23}$ (bacterial killing), $\alpha_8$ and $c_8$ (phagocytosis), and $N_c$ by 40% resulting in 99.47% of clearance cases.

## Discussion

To our knowledge, ours is the first study to develop a mathematical model representing immune system and bacterial dynamics during *Salmonella* infection at an organ (MLN) level. The model predicted three different disease trajectories, namely clearance, active disease and latency, with accurate percent estimation of each. For active disease and latency cases, we observed a lag before the bacterial population starts to increase. This interval can be classified as an

Downloaded from https://academic.oup.com/intimm/article/33/5/281/6066543 by guest on 27 December 2022

incubation period after which the disease symptoms start appearing and is concurrent with the observed lag in the detection of bacteria in the MLN of infected mice (53).

We reliably explored and validated the cellular and cytokine dynamics operational during different disease outcomes of murine typhoid. In accordance with the literature (27), the model accurately predicted a $T_{H1}$-biased immune response during active disease and a $T_{H2}$ bias during latency. The $M_1$ (pro-inflammatory macrophages) and $T_{H1}$-biased immune response during active disease is indicative of tissue damage. Further, as reported elsewhere (4, 13), during latency, more than 80% of the bacteria were associated with macrophages at the end of the 100th day (Fig. 2). The results of virtually implemented therapeutic strategies also confirm these intra-macrophage *Salmonella* as the source of persistent infection. Moreover, the persistent infection is hard to cure completely without critically reducing the $M_0$ and $M_2$ macrophage populations. Supplementary to this, we observe higher IFN-γ during latency and active disease (Fig. 4). With support from the literature (4, 8, 58), we propose that, higher IFN-γ helps in containing the bacterial number during latency perhaps by sustaining threshold concentration of anti-bacterial $M_1$ macrophages and $DC_m$, while controlling the pro-bacterial $M_2$ macrophage number (Fig. 3). Likewise, the model predicts that suppressing IFN-γ increases the proportion of $M_2$ macrophages re-activating the latency cases (Table 1). This again highlights the importance of inflammatory (high $T_{H1}$ and IFN-γ) response in controlling the disease.

However, the results of virtual deletion experiments indicate that the $T_{H1}/T_{H2}$ balance and inflammatory response are not the only factors determining the outcome of *Salmonella* infection. The bacterial potency may also have a role to play. The infection studies with mice having a $T_{H1}$ (C57BL/6) or $T_{H2}$ (BALB/c) biased immune response do not show stark difference in infection outcome (59), thus confirming our prediction.

As per the virtual deletion analysis, the entire system does not progress to active disease on IL-12 or IFN-γ (inflammatory cytokines) deletion. On the other hand, the virtual depletion of these cytokines leads to reactivation of almost all latency cases by the 150th day. IL-12 is indicated to have a complementary role in controlling *Salmonella* number within the host (43, 60). It manifests its effects by inducing the production of IFN-γ by neutrophils, T cells and NK cells, a major source of IFN-γ (43, 60). Accordingly, our model predicts fewer active disease cases with IL-12 deletion/depletion than that with IFN-γ deletion/depletion (Table 1). The results of deletion and depletion experiments signify that along with the inflammatory response, the bacterial potential also influences the disease progression. The global SA further testifies this (Table 2). The weightage of bacterial parameters in governing the disease progression is increased during the later phase of infection. We assume that the bacteria causing latency in healthy individuals are potent enough to cause active disease on suppressing the host inflammatory response. They are also sufficiently tolerant to the inflammatory response, thereby preventing their clearance from the system. Correspondingly, very few latency cases (1%) are cured on depleting IL-4 (which increases the inflammatory response). The results of virtual deletion and depletion experiments also signify the importance of the initial inflammatory response in controlling the disease. A higher inflammatory response ($T_{H1}$ bias and IFN-γ) in the initial period (as with IL-4 deletion) increases incidences of clearance (by ~25%), while the absence (as with IFN-γ deletion) increases the incidences of active disease (by ~50–60%, Table 1). A $T_{H2}$-biased immune response was also observed in reactivation and re-infection cases.

Furthermore, global SA confirms the importance of the inflammatory response. Some parameters like $\alpha_{35}$ are important in the initial phase of the disease, while those like $c_{17}$ are important in the later phase. This can be justified through the importance of $T_{H1}$ cells in resolving primary *Salmonella* infection by producing IFN-γ at rate $\alpha_{35}$. Further support is gathered through the fact that patients with HIV infection who lack $T_H$ cells are highly susceptible to *Salmonella* infection and the anti-retroviral therapy restoring the $T_H$ cells reduces the susceptibility of the patients (40). IFN-γ is also important for containing the bacteria during latency, further explaining the importance of $c_{17}$ in the later half. The $c_{17}$ parameter regulates IL-12 production by $M_0$ and $M_1$ macrophages; IL-12 further governs the IFN-γ secretion by neutrophils, NK and T cells ($s_{10}$ term, Equation 15 in Supplementary Methods). Almost all top 15 parameters identified through SA are included directly or indirectly in the RoM. The equations of the RoM comprehend most of the key mechanisms deemed important through SA accurately predicting the disease outcome with minor deviations from the full-order model.

As per the model predictions, better prophylaxis is obtained by controlling the growth rate of extracellular ($\alpha_{23}$) but not of intracellular bacteria ($\alpha_{24}$ and $\alpha_{26}$, Table 2). In addition, when we affected the bacterial growth rate, we observed a 5–10% chronic carriage rate pursuant to epidemiological data on typhoid (54), thus endorsing the non-growing intra-macrophage persisters as the potential source of relapse (9). Global SA highlighted the prominence of both the bacterial and the host attributes in governing disease progression. The replication potential (captured by $\alpha_{23}$) of *Salmonella* is the most influential attribute governing the progress of disease. The model suggests that the phagocytic and anti-microbial potential of the phagocytes (macrophages and DCs) and IFN-γ concentration are fundamental in controlling the infection. This illustrates the importance of a strong innate immune response in controlling typhoid. Affecting the parameters ($\alpha_8$, $c_8$, $\mu_{16}$, $\gamma$, $s_1$ and $c_3$) associated with these attributes significantly reduced active disease cases but with 9–16% of latency cases. Targeting these parameters could be considered as a potential therapeutic strategy against antibiotic-resistant strains. For instance, IFN-γ therapy, adoptive DC transfer and drugs to improve phagocytic potential of macrophages can be considered as potential alternative therapeutic strategies (Tables 2 and 3).

The inefficiency of current therapeutic strategies (incomplete cure with 3–12% latency cases) (27) and emergence of anti-microbial resistance in *Salmonella*, especially in South and Southeast Asia (majorly from India, Nepal, Bangladesh and Vietnam) and Africa (Sub-Saharan, East and Southwest regions), pose a daunting threat due to limited options (55, 56). Third-generation cephalosporins are used for typhoidal treatment in South and Southeast Asia (55). However, ~4% of isolates from these regions are resistant to these drugs (55). Under such a scenario, vaccine development seems

Downloaded from https://academic.oup.com/intimm/article/33/5/281/6066543 by guest on 27 December 2022

an effective alternative strategy to prevent infections in developing countries with endemic typhoid fever (55, 56) and travelers (from developed countries) visiting these nations. The results of our virtual prevention strategies simulating effects equivalent to vaccination (36–38, 57) confirm this. The incidences of latency were reduced up to ~2% (2–13%) and the clearance cases increased to greater than 85% (85–98%), which is close to the protective efficacy of the current vaccines or those in the pipeline (56, 57). The simulation results indicate that a vaccine (i) eliciting a robust long-lasting humoral immune response (equivalent to decreasing $\alpha_{23}$ and $c_8$ while increasing $\alpha_8$) and (ii) increasing the macrophage carrying capacity or its killing potential and IFN-γ half-life would be highly potent in preventing (>99%) the occurrence of typhoid in vaccinated individuals (Table 3). These attributes can be considered as targets in developing effective vaccine in countries with endemic typhoid fever—for instance, a conjugate vaccine consisting of a strong antigen to induce a strong humoral immune response. We propose that a vaccine with an ability to shift the parameters corresponding to above-mentioned attributes by at least 45% may prove to be highly effective.

## Funding

This work was supported by the Department of Science and Technology–Science and Engineering Research Board, India (EMR/2014/001246 to S.A.M., A.M. and D.C.).

## Acknowledgements

We thank Ms. Poorvi Raghvendra and Vivek Gurung for helping in experiments pertaining to parameter estimation. S.A.M. conceived the idea and designed the study. S.A.M., D.D. A.M. and N.S. performed the experiments. S.A.M., D.D. and A.M. interpreted the data as well as wrote the paper. S.A.M., D.D., A.M. and D.C. reviewed the manuscript. All authors approved the final manuscript.

*Conflicts of interest statement:* the authors declared no conflicts of interest.

## References

1 Stanaway, J. D., Reiner, R. C., Blacker, B. F. *et al*. 2019. The global burden of typhoid and paratyphoid fevers: a systematic analysis for the Global Burden of Disease Study 2017. *Lancet Infect. Dis*. 19:369.
2 Parry, C. M., Hien, T. T., Dougan, G., White, N. J. and Farrar, J. J. 2002. Typhoid fever. *N. Engl. J. Med*. 347:1770.
3 Higginson, E. E., Simon, R. and Tennant, S. M. 2016. Animal models for salmonellosis: applications in vaccine research. *Clin. Vaccine Immunol*. 23:746.
4 Monack, D. M., Bouley, D. M. and Falkow, S. 2004. *Salmonella typhimurium* persists within macrophages in the mesenteric lymph nodes of chronically infected Nramp1$^{+/+}$ mice and can be reactivated by IFNgamma neutralization. *J. Exp. Med*. 199:231.
5 Voedisch, S., Koenecke, C., David, S. *et al*. 2009. Mesenteric lymph nodes confine dendritic cell-mediated dissemination of *Salmonella enterica* serovar Typhimurium and limit systemic disease in mice. *Infect. Immun*. 77:3170.
6 Helaine, S., Cheverton, A. M., Watson, K. G., Faure, L. M., Matthews, S. A. and Holden, D. W. 2014. Internalization of *Salmonella* by macrophages induces formation of nonreplicating persisters. *Science* 343:204.
7 Thiriot, J. D., Martinez-Martinez, Y. B., Endsley, J. J. and Torres, A. G. 2020. Hacking the host: exploitation of macrophage polarization by intracellular bacterial pathogens. *Pathog. Dis*. 78:ftaa009.
8 Eisele, N. A., Ruby, T., Jacobson, A. *et al*. 2013. *Salmonella* require the fatty acid regulator PPARδ for the establishment of a metabolic environment essential for long-term persistence. *Cell Host Microbe* 14:171.
9 Stapels, D. A. C., Hill, P. W. S., Westermann, A. J. *et al*. 2018. *Salmonella* persisters undermine host immune defenses during antibiotic treatment. *Science* 362:1156.
10 Nakahara, T., Urabe, K., Fukagawa, S. *et al*. 2005. Engagement of human monocyte-derived dendritic cells into interleukin (IL)-12 producers by IL-1beta + interferon (IFN)-gamma. *Clin. Exp. Immunol*. 139:476.
11 Murray, P. J., Allen, J. E., Biswas, S. K. *et al*. 2014. Macrophage activation and polarization: nomenclature and experimental guidelines. *Immunity* 41:14.
12 McSorley, S. J. 2014. Immunity to intestinal pathogens: lessons learned from *Salmonella*. *Immunol. Rev*. 260:168.
13 Ruby, T., McLaughlin, L., Gopinath, S. and Monack, D. 2012. *Salmonella*'s long-term relationship with its host. *FEMS Microbiol. Rev*. 36:600.
14 Kaiser, P., Slack, E., Grant, A. J., Hardt, W. D. and Regoes, R. R. 2013. Lymph node colonization dynamics after oral *Salmonella* Typhimurium infection in mice. *PLoS Pathog*. 9:e1003532.
15 Kaiser, P., Regoes, R. R., Dolowschiak, T. *et al*. 2014. Cecum lymph node dendritic cells harbor slow-growing bacteria phenotypically tolerant to antibiotic treatment. *PLoS Biol*. 12:e1001793.
16 Grant, A. J., Restif, O., McKinley, T. J., Sheppard, M., Maskell, D. J. and Mastroeni, P. 2008. Modelling within-host spatiotemporal dynamics of invasive bacterial disease. *PLoS Biol*. 6:e74.
17 Griffin, A. J., Li, L. X., Voedisch, S., Pabst, O. and McSorley, S. J. 2011. Dissemination of persistent intestinal bacteria via the mesenteric lymph nodes causes typhoid relapse. *Infect. Immun*. 79:1479.
18 Rydström, A. and Wick, M. J. 2007. Monocyte recruitment, activation, and function in the gut-associated lymphoid tissue during oral *Salmonella* infection. *J. Immunol*. 178:5789.
19 Mège, J. L., Mehraj, V. and Capo, C. 2011. Macrophage polarization and bacterial infections. *Curr. Opin. Infect. Dis*. 24:230.
20 Bravo-Blas, A., Utriainen, L., Clay, S. L. *et al*. 2019. *Salmonella enterica* serovar typhimurium travels to mesenteric lymph nodes both with host cells and autonomously. *J. Immunol*. 202:260.
21 Guiney, D. G. 2005. The role of host cell death in *Salmonella* infections. *Curr. Top. Microbiol. Immunol*. 289:131.
22 Sundquist, M. and Wick, M. J. 2009. *Salmonella* induces death of CD8alpha(+) dendritic cells but not CD11c(int)CD11b(+) inflammatory cells *in vivo* via MyD88 and TNFR1. *J. Leukoc. Biol*. 85:225.
23 Lapaque, N., Walzer, T., Méresse, S., Vivier, E. and Trowsdale, J. 2009. Interactions between human NK cells and macrophages in response to *Salmonella* infection. *J. Immunol*. 182:4339.
24 Marino, S. and Kirschner, D. E. 2004. The human immune response to *Mycobacterium tuberculosis* in lung and lymph node. *J. Theor. Biol*. 227:463.
25 Yrlid, U., Svensson, M., Håkansson, A., Chambers, B. J., Ljunggren, H. G. and Wick, M. J. 2001. *In vivo* activation of dendritic cells and T cells during *Salmonella* enterica serovar Typhimurium infection. *Infect. Immun*. 69:5726.
26 Johansson, C. and Wick, M. J. 2004. Liver dendritic cells present bacterial antigens and produce cytokines upon *Salmonella* encounter. *J. Immunol*. 172:2496.
27 Gal-Mor, O. 2019. Persistent infection and long-term carriage of typhoidal and nontyphoidal *Salmonellae*. *Clin. Microbiol. Rev*. 32:e00088–18.
28 Pietilä, T. E., Veckman, V., Kyllönen, P., Lähteenmäki, K., Korhonen, T. K. and Julkunen, I. 2005. Activation, cytokine production, and intracellular survival of bacteria in *Salmonella*-infected human monocyte-derived macrophages and dendritic cells. *J. Leukoc. Biol*. 78:909.
29 Hochrein, H., Shortman, K., Vremec, D., Scott, B., Hertzog, P., and O'Keeffe, M. 2001. Differential production of IL-12, IFN-α, and IFN-γ by mouse dendritic cell subsets. *J. Immunol*. 166:5448.

Downloaded from https://academic.oup.com/intimm/article/33/5/281/6066543 by guest on 27 December 2022

30 Yrlid, U. and Wick, M. J. 2002. Antigen presentation capacity and cytokine production by murine splenic dendritic cell subsets upon *Salmonella* encounter. *J. Immunol.* 169:108.
31 Wigginton, J. E. and Kirschner, D. 2001. A model to predict cell-mediated immune regulatory mechanisms during human infection with *Mycobacterium tuberculosis*. *J. Immunol.* 166:1951.
32 Blower, S. M. and Dowlatabadi, H. 1994. Sensitivity and uncertainty analysis of complex models of disease transmission: an HIV model, as an example. *Int. Stat. Rev.* 62:229.
33 Marino, S., Hogue, I. B., Ray, C. J. and Kirschner, D. E. 2008. A methodology for performing global uncertainty and sensitivity analysis in systems biology. *J. Theor. Biol.* 254:178.
34 Kirschner, D. 2007. Uncertainty and sensitivity functions and implementation. http://malthus.micro.med.umich.edu/lab/usadata.
35 Wangersky, P. J. 1978. Lotka-volterra population models. *Ann. Rev. Ecol. Systemat.* 9:189.
36 Wahid, R., Zafar, S. J., McArthur, M. A., Pasetti, M. F., Levine, M. M. and Sztein, M. B. 2014. Live oral *Salmonella enterica* serovar Typhi vaccines Ty21a and CVD 909 induce opsonophagocytic functional antibodies in humans that cross-react with *S.* Paratyphi A and *S.* Paratyphi B. *Clin. Vaccine Immunol.* 21:427.
37 Simon, R., Tennant, S. M., Wang, J. Y. *et al.* 2011. *Salmonella enterica serovar* enteritidis core O polysaccharide conjugated to H:g,m flagellin as a candidate vaccine for protection against invasive infection with *S.* enteritidis. *Infect. Immun.* 79:4240.
38 Baliban, S. M., Allen, J. C., Curtis, B. *et al.* 2018. Immunogenicity and induction of functional antibodies in rabbits immunized with a trivalent typhoid-invasive nontyphoidal. *Molecules* 23:1749.
39 Blohmke, C. J., Hill, J., Darton, T. C. *et al.* 2017. Induction of cell cycle and NK cell responses by live-attenuated oral vaccines against typhoid fever. *Front. Immunol.* 8:1276.
40 Kurtz, J. R., Goggins, J. A. and McLachlan, J. B. 2017. *Salmonella* infection: interplay between the bacteria and host immune system. *Immunol. Lett.* 190:42.
41 Eckmann, L., Fierer, J. and Kagnoff, M. F. 1996. Genetically resistant (Ityr) and susceptible (Itys) congenic mouse strains show similar cytokine responses following infection with *Salmonella dublin*. *J. Immunol.* 156:2894.
42 De Jong, H. K., Koh, G. C., van Lieshout, M. H. *et al.* 2014. Limited role for ASC and NLRP3 during *in vivo Salmonella* Typhimurium infection. *BMC Immunol.* 15:30.
43 Mastroeni, P., Harrison, J. A., Chabalgoity, J. A. and Hormaeche, C. E. 1996. Effect of interleukin 12 neutralization on host resistance and gamma interferon production in mouse typhoid. *Infect. Immun.* 64:189.
44 Wenzel, U. A., Fernandez-Santoscoy, M., Tam, M. A., Tegtmeyer, P. and Wick, M. J. 2015. Synergy between CD40 and MyD88 does not influence host survival to *Salmonella* Infection. *Front. Immunol.* 6:460.
45 Brown, D. E., Libby, S. J., Moreland, S. M. *et al.* 2013. *Salmonella enterica* causes more severe inflammatory disease in C57/BL6 Nramp1G169 mice than Sv129S6 mice. *Vet. Pathol.* 50:867.
46 Depaolo, R. W., Lathan, R., Rollins, B. J. and Karpus, W. J. 2005. The chemokine CCL2 is required for control of murine gastric *Salmonella enterica* infection. *Infect. Immun.* 73:6514.
47 Fernández-Santoscoy, M., Wenzel, U. A., Yrlid, U., Cardell, S., Bäckhed, F. and Wick, M. J. 2015. The gut microbiota reduces colonization of the mesenteric lymph nodes and IL-12-Independent IFN-γ production during *Salmonella* infection. *Front. Cell. Infect. Microbiol.* 5:93.
48 O'Mahony, L., O'Callaghan, L., McCarthy, J. *et al.* 2006. Differential cytokine response from dendritic cells to commensal and pathogenic bacteria in different lymphoid compartments in humans. *Am. J. Physiol. Gastrointest. Liver Physiol.* 290:G839–G845.
49 Ramirez-Alejo, N. and Santos-Argumedo, L. 2014. Innate defects of the IL-12/IFN-γ axis in susceptibility to infections by mycobacteria and salmonella. *J. Interferon Cytokine Res.* 34:307.
50 Jouanguy, E., Döffinger, R., Dupuis, S., Pallier, A., Altare, F. and Casanova, J. L. 1999. IL-12 and IFN-gamma in host defense against mycobacteria and *Salmonella* in mice and men. *Curr. Opin. Immunol.* 11:346.
51 Meltzer, E. and Schwartz, E. 2007. Enteric fever: an Israeli perspective. *Isr. Med. Assoc. J.* 9:736.
52 Sundquist, M. and Wick, M. J. 2005. TNF-alpha-dependent and -independent maturation of dendritic cells and recruited $CD11c^{(int)}CD11b^{+}$ cells during oral *Salmonella* infection. *J. Immunol.* 175:3287.
53 Awofisayo-Okuyelu, A., McCarthy, N., Mgbakor, I. and Hall, I. 2018. Incubation period of typhoidal salmonellosis: a systematic review and meta-analysis of outbreaks and experimental studies occurring over the last century. *BMC Infect. Dis.* 18:483.
54 Gunn, J. S., Marshall, J. M., Baker, S., Dongol, S., Charles, R. C. and Ryan, E. T. 2014. *Salmonella* chronic carriage: epidemiology, diagnosis, and gallbladder persistence. *Trends Microbiol.* 22:648.
55 Britto, C. D., Wong, V. K., Dougan, G. and Pollard, A. J. 2018. A systematic review of antimicrobial resistance in *Salmonella enterica* serovar Typhi, the etiological agent of typhoid. *PLoS Negl. Trop. Dis.* 12:e0006779.
56 Marathe, S. A., Lahiri, A., Negi, V. D. and Chakravortty, D. 2012. Typhoid fever & vaccine development: a partially answered question. *Indian J. Med. Res.* 135:161.
57 Baliban, S. M., Lu, Y. J. and Malley, R. 2020. Overview of the nontyphoidal and paratyphoidal *salmonella* vaccine pipeline: current status and future prospects. *Clin. Infect. Dis.* 71(suppl. 2):S151.
58 Ingram, J. P., Brodsky, I. E. and Balachandran, S. 2017. Interferon-γ in *Salmonella* pathogenesis: new tricks for an old dog. *Cytokine* 98:27.
59 Ma, Y., Chen, H., Wang, Q., Luo, F., Yan, J. and Zhang, X. L. 2009. IL-24 protects against *Salmonella typhimurium* infection by stimulating early neutrophil $T_h1$ cytokine production, which in turn activates $CD8^{+}$ T cells. *Eur. J. Immunol.* 39:3357.
60 John, B., Rajagopal, D., Pashine, A., Rath, S., George, A. and Bal, V. 2002. Role of IL-12-independent and IL-12-dependent pathways in regulating generation of the IFN-gamma component of T cell responses to *Salmonella typhimurium*. *J. Immunol.* 169:2545.

Downloaded from https://academic.oup.com/intimm/article/33/5/281/6066543 by guest on 27 December 2022